The Nature of Quasicleavage Fracture in Tempered 5.5Ni Steel after Hydrogen Charging

Y. H. KIM and J.W. MORRIS, Jr.

Quenched and tempered 5.5Ni steel was embrittled by hydrogen charging and broken in air at room temperature. The primary fracture mode was transgranular quasicleavage. The quasicleavage facets were studied by scanning electron fractography and by transmission electron microscopy of profile fractographic specimens. The latter were prepared by plating the fracture surface with nickel and thinning so that the fracture surface was contained within the region of the specimen that was transparent to the electron beam. The fracture surface generally followed martensite lath boundaries. In addition, interlath microcracks were frequently found in the material immediately beneath the fracture surface. These results suggest that transgranular hydrogen embrittlement in this steel is primarily an interlath cracking phenomenon. Since the lath boundary planes tend to lie in {110}, the results also explain the prevalence of {110} quasicleavage in the embrittled specimens, which contrasts with the {100} cleavage found in uncharged specimens broken below the ductile-to-brittle transition temperature.

I. INTRODUCTION

WHEN high strength martensitic steels are embrittled by hydrogen they may fail either by intergranular separation along the prior austenite grain boundaries or by transgranular fracture along planes which traverse the prior austenite grains. The transgranular failure mode superficially resembles the transgranular cleavage fracture found in similar steels when they are broken below their ductile-to-brittle transition temperatures. Recent research has shown, however, that there are significant differences. The most striking of these is the fracture plane itself, which is predominantly {100} in low-temperature fracture, but is often found to be {110} or {112} after hydrogen embrittlement.[1-4] While the {100} plane is the natural cleavage plane in bcc iron, the {110} and {112} are the dominant slip planes.

The coincidence between the fracture plane and the dominant slip plane in steels that have been embrittled by hydrogen has led several authors to suggest that embrittlement occurs through a "glide plane decohesion" resembling that occasionally found in the basal plane fracture of hexagonal close-packed metals.[1,2,5,6] The evidence supporting this hypothesis is indirect, however, and there is an alternative explanation for the crystallography of transgranular fracture which is based on the prevalence of {110} and {112} planes in the boundaries of martensite plates and subgrains in high strength steel. The {110} plane is the usual low angle boundary plane separating laths in lath martensitic steels; the {112} plane is the boundary plane when adjacent laths are twin-related.[7,8] Both the {110} and {112} planes are common boundary planes for the subgrains formed in iron after severe deformation or tempering.[9] It is therefore possible that transgranular fracture in embrittled high strength steels follows lath or subgrain boundaries, and hence resembles intergranular fracture more than either transgranular cleavage or glide plane decohesion.

To clarify this issue we carried out high resolution studies of the fracture path in a 5.5Ni steel which had been embrittled by hydrogen charging. 5.5Ni is a high alloy steel that is sold commercially for structural use at cryogenic temperatures. Its microstructure is well known, and typically contains well-defined laths of dislocated martensite that are organized into packets (Figure 1). The laths within a packet are separated by highly dislocated, low angle boundaries that tend to follow {110} planes (Figure 2).[7] Below its ductile-to-brittle transition temperature 5.5Ni steel fractures in a brittle transgranular mode along {100} cleavage planes.[7,8] Since the microstructure and mechanical properties of 5.5Ni steel are well known and techniques have been developed for high resolution studies of its transgranular fracture features, this alloy seemed a natural candidate for research on transgranular hydrogen embrittlement.

II. EXPERIMENTAL PROCEDURE

The alloy used in this study was a commercial 5.5Ni steel provided by the Nippon Steel Corporation. The alloy was supplied as a 35 mm plate. Its composition was determined

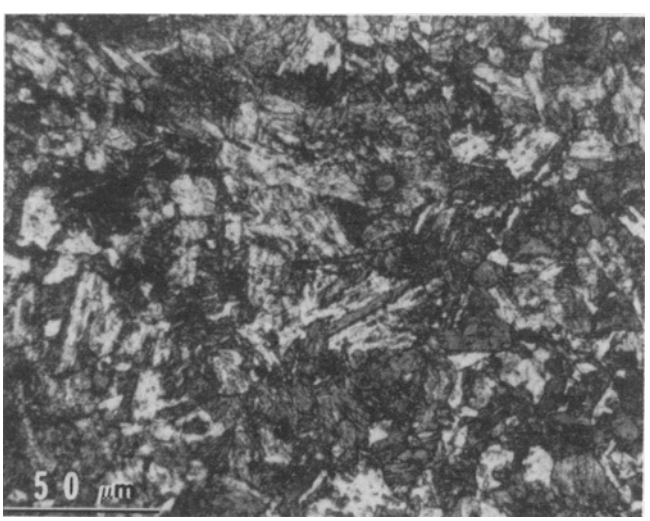

Fig. 1—Optical micrograph of quenched and tempered 5.5Ni steel.

Y. H. KIM, Graduate Research Assistant, Lawrence Berkeley Laboratory, and J.W. MORRIS, Jr., Professor, are both with the University of California, Berkeley, CA 94720.

Manuscript submitted November 16, 1982.

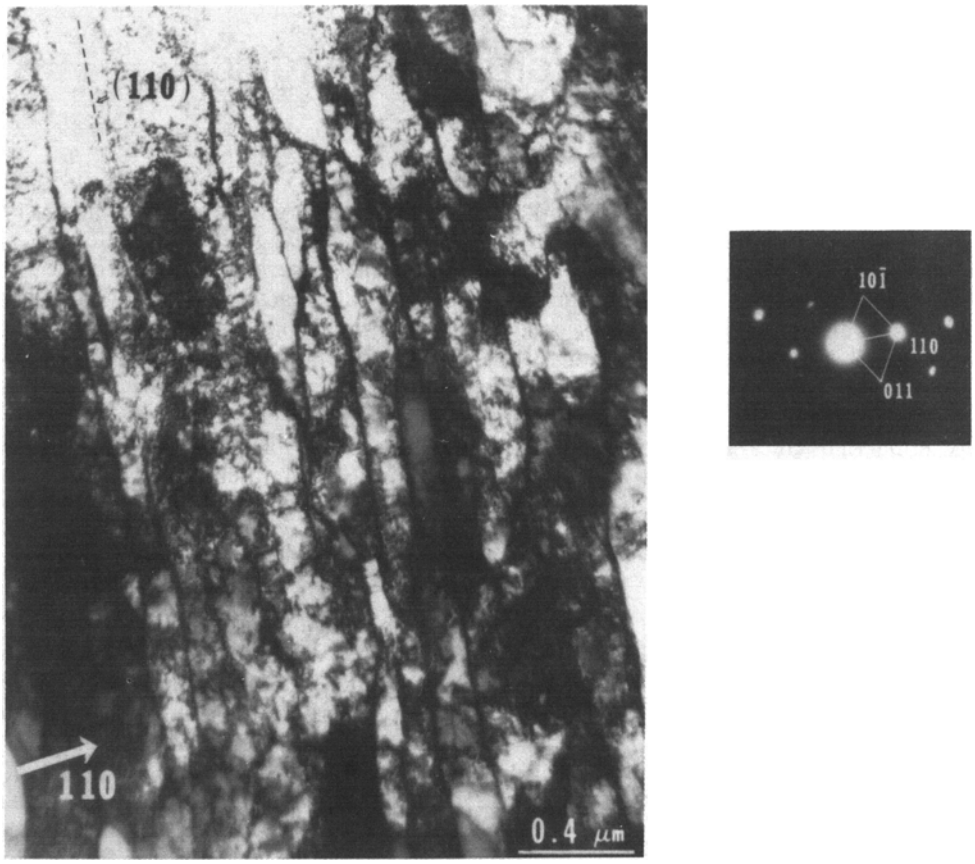

Fig. 2—Transmission electron micrograph showing the appearance of martensite laths in tempered 5.5Ni steel.

to be: Fe-5.86Ni-1.21Mn-0.69Cr-0.2Mo-0.2Si-0.06C-0.01S-0.008P (in weight percent). The alloy was annealed at 1200 °C for two hours to remove the effects of prior treatment, and then given a quench and temper treatment to eliminate any tendency toward fracture along the prior austenite grain boundaries. It was austenitized at 800 °C for one hour, water quenched, and tempered at 600 °C for one hour. Standard sized charpy impact specimens were cut from the tempered plate, fatigue precracked, and fractured slowly in three-point bending.

Specimens were cathodically charged in 1N H_2SO_4 using a platinum sheet anode. Small amounts of As_2O_3 and CS_2 were added to the electrolyte to prevent recombination of hydrogen gas.[3] The specimens were precharged for 24 hours at a current density of 100 milliamps per square centimeter, and were fractured at room temperature in air within two minutes after completion of the charging.

Fractographic analyses of the broken specimens included optical and scanning electron microscopy to determine the fracture mode, chemical etching to identify the quasicleavage plane,[1] and transmission electron microscopy on "profile fractographic"[10,11] specimens to observe the fracture plane and the associated subsurface damage. The chemical etching was done using the three-step procedure and the reagent suggested by Matsuda, *et al.*[12] The profile fractographic specimens were prepared by electroplating the fracture surface with nickel and then slicing the specimen along the direction of crack propagation and perpendicular to the fracture surface. After mechanical polishing to reduce thickness, thin foil specimens were prepared by a combination of electropolishing and ion beam milling.[13] A number of foils were obtained which contained the profile of the fracture surface within the region that was transparent to 100 kV electrons. The foils were then examined in a transmission electron microscope at an operating voltage of 100 kV.

III. RESULTS

A. *Microstructure*

The microstructure of the tempered specimens is illustrated in Figures 1 and 2. The microstructure consists of packets of dislocated martensite laths. The laths within a packet are usually separated by highly dislocated low angle boundaries which lie nearly parallel to {110} planes (Figure 2). Twin boundaries along {112} planes and high angle boundaries are also occasionally found. As a consequence of tempering, the dislocations within the laths are partially polygonized into subgrains. The tempering temperature, 600 °C, is slightly within the intercritical range. There is hence some retained austenite in the microstructure, which X-ray analysis shows to be approximately 2 pct by volume, and there are occasional fresh martensite laths that are due to the retransformation of austenite formed during tempering.

B. *Mechanical Test Results*

Figure 3 shows typical load-deflection curves for 3-point bending specimens fractured with and without hydrogen charging. The hydrogen-free specimen had a high fracture toughness, approximately 330 MPa · $m^{1/2}$ (300 ksi · $in^{1/2}$), and fractured in a totally ductile manner as illustrated by the scanning electron fractographs presented in Figure 4. Hydrogen charging caused a drop in the load-deflection curve and a substantial decrease in the fracture toughness to approximately 180 MPa · $m^{1/2}$ (160 ksi · $in^{1/2}$). In this case, also, the sample was significantly deformed during fracture. The primary fracture mode was quasicleavage (Figure 5), with an occasional admixture of ductile rupture. Secondary quasicleavage cracks were observed branching away from the fracture surface.

C. *Detailed Analysis of Quasicleavage Fracture*

A close examination of scanning electron fractographs of the hydrogen-embrittled specimens (for example, Figure 5) reveals that the quasicleavage portions of the fracture surface are decorated by fine, lath-like features which are comparable in dimension to the martensite laths shown in Figure 2. The etch pits formed on these surfaces (Figure 6) show the elongated-hexagon shape which is typical of etch pits on {110} surfaces.[1,2] These observations suggest that the fracture propagates preferentially along the martensite laths, and lies either in or parallel to the lath boundaries. Optical and scanning electron micrographs of etched fracture profile specimens (for example, Figure 7) confirm this conclusion, and suggest that the predominant fracture mode is lath boundary separation.

Transmission electron micrographs of the profile fractographic specimens afford a more detailed view of the fracture surface and the immediate subsurface region. Four example micrographs are presented in Figures 8(a) to (d). There is some uncertainty in the precise location of the fracture surface since the matching surface is unavailable and since it is possible that the specimen surface was slightly altered by the plating process. It is clear, however, that the fracture surface tends to parallel the long axis of the martensite laths. It also appears that the fracture surface lies in the lath boundaries over almost its whole length. Its probable deviations from the lath boundary, for example, the segments marked with an asterisk at the lower right in Figure 8(d), seem to represent short steps connecting longer segments of interlath fracture. The material immediately beneath the fracture surface sometimes has a simple diffraction pattern, showing that it is a single martensite packet which has not been severely deformed. In this case, which is exemplified by Figures 8(b) and (d), the plane of fracture can be identified and is close to {110}. Other subsurface regions yield diffraction patterns in which the spots are spread into arcs along the diffraction circle, as in Figure 8(a). These regions were evidently deformed during fracture.

The high resolution transmission electron fractographs also reveal a dense population of fine secondary cracks immediately beneath the fracture surface. These secondary microcracks are present in all micrographs; they are located by solid arrows in Figure 8. The microcracks are almost

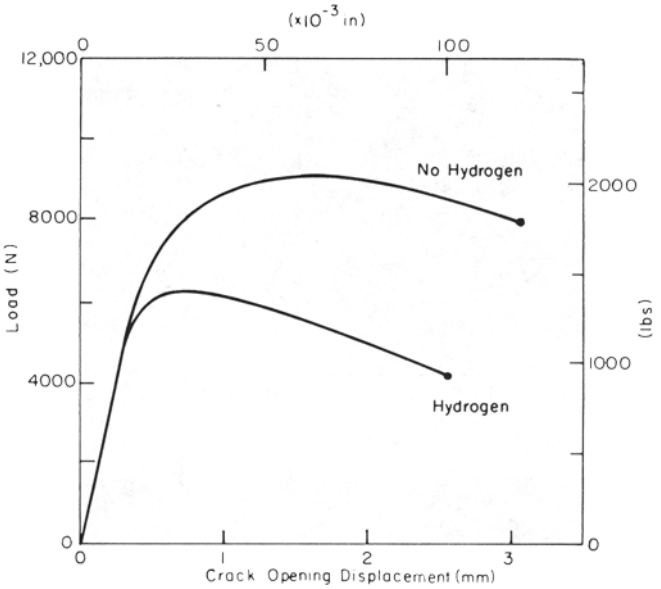

Fig. 3 — The load-displacement curves of 3-point bend specimens of 5.5Ni steel tested before and after hydrogen charging.

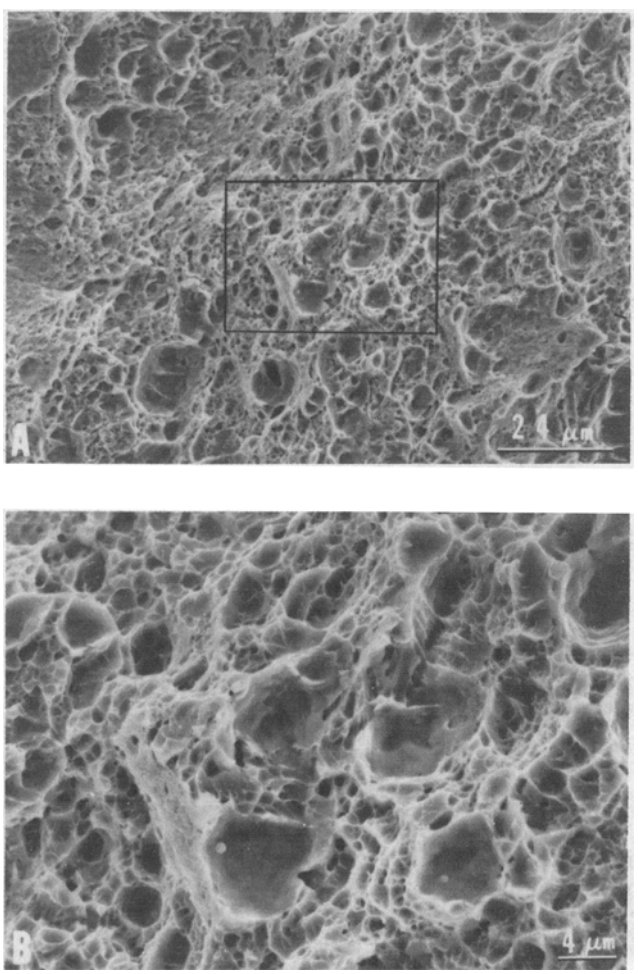

Fig. 4 — Scanning electron fractographs of a 3-point bend specimen broken in the uncharged condition. (*a*) Low magnification fractograph showing the ductile rupture fracture mode. (*b*) Higher magnification view of the region outlined in (a).

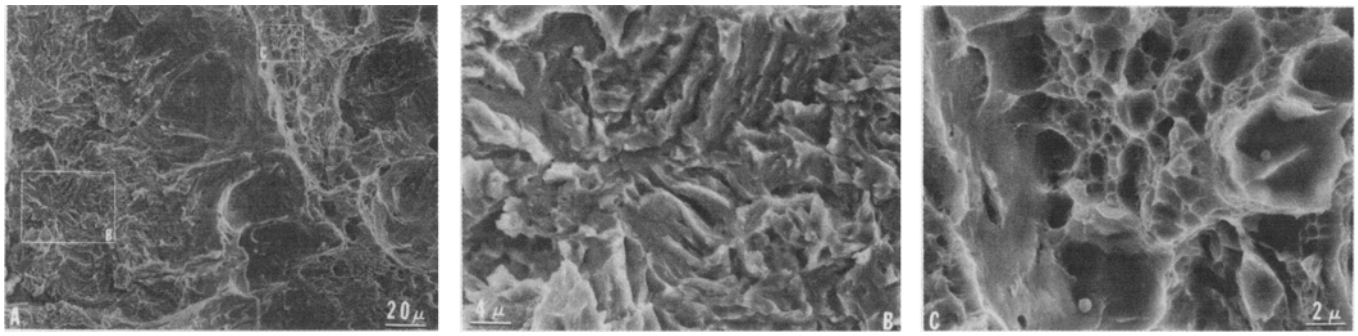

Fig. 5 — Scanning electron fractographs of a 3-point bend specimen broken after hydrogen charging. (*a*) Low magnification fractograph showing the presence of quasicleavage fracture. (*b*) High magnification view of the quasicleavage fracture surface. (*c*) High magnification view of a region of ductile fracture.

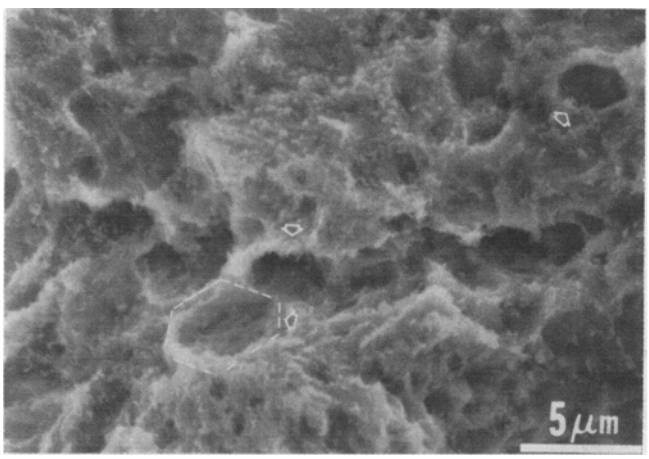

Fig. 6 — Scanning electron micrograph of the quasicleavage fracture surface after 3-step etching with the reagent proposed in Ref. 12. The outlined etch pit has a shape indicating a fracture plane near {110}.

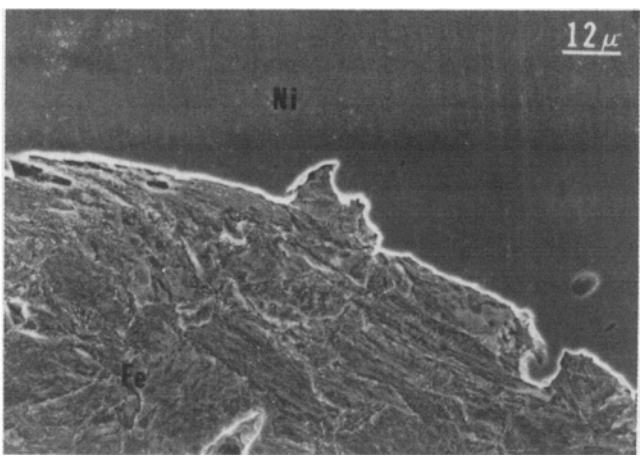

Fig. 7 — Scanning electron micrograph of the fracture surface in the specimen embrittled by hydrogen. The specimen has been etched to reveal the lath structure.

certainly associated with the fracture process since they are commonly found in the first few micrometers of material beneath the fracture surface, but are not found in specimens taken from deeper within the fractured sample. The secondary microcracks almost invariably lie in and along lath boundaries. They usually initiate at irregularities in the lath boundary such as boundary intersections, steps, or foreign particles, and continue as sharp flaws in the boundary plane. In one isolated instance, shown in Figure 8(c), a microcrack was located in the interior of a lath. This microcrack emanates from an impurity particle which is probably a carbide.

IV. DISCUSSION AND CONCLUSION

The results presented above strongly suggest that the quasicleavage fracture associated with hydrogen embrittlement in 5.5Ni steel is predominantly interlath fracture. The evidence supporting this conclusion includes the following: (1) The superficial quasicleavage plane is the common lath boundary plane. (2) All optical, scanning, and transmission electron micrographic views of the fracture surface reveal an apparent interlath fracture. (3) Interlath microcracks are common in the material immediately beneath the fracture surface. (4) Translath fracture segments are only occasionally found, and seem to be either internal microcracks due to impurity particles or short steps connecting interlath features. Hydrogen-induced transgranular quasicleavage hence appears to be an interlath phenomenon which phenomenalogically resembles intergranular fracture.

The results also suggest a mechanism for hydrogen-induced quasicleavage: interlath microcracks nucleate in the stressed region ahead of the crack tip at irregularities in the lath boundaries, propagate along the boundaries, and eventually link together, sometimes across laths, to form the macroscopic fracture surface. Several observations support this interpretation. The interlath microcracks near the fracture surface almost certainly form ahead of the propagating crack tip, since the stress required to nucleate them would be relieved once the crack tip had passed. The transmission electron fractographs contain clear evidence for microcrack propagation along lath boundaries. The continuity of the lath boundary network permits the growing microcracks to link together; parallel microcracks may also link by shearing the intervening bulk material. This mechanism explains both the {110} quasicleavage plane and the microscopic roughness of the quasicleavage fracture surface, which is an expected consequence of the irregularities in both the lath boundary network and the microcrack nucleation process. While the {112} quasicleavage plane was not found in the limited number of micrographs examined in the present work, {112} facets can also arise from interlath fracture since {112} boundaries

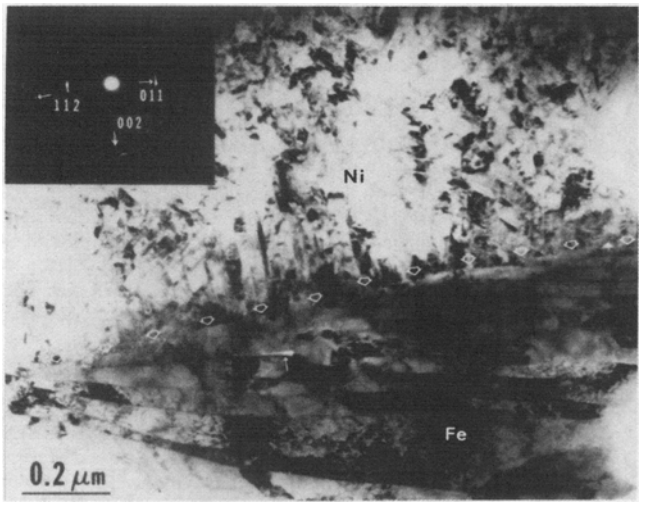

(a)

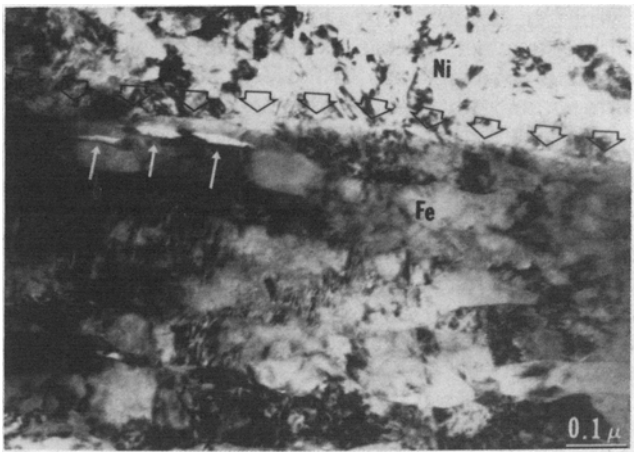

(b)

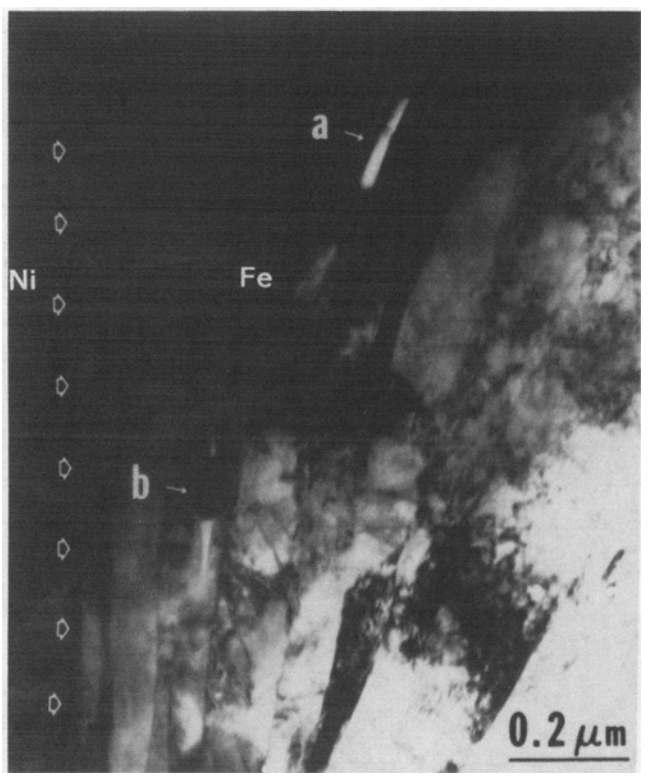

(c)

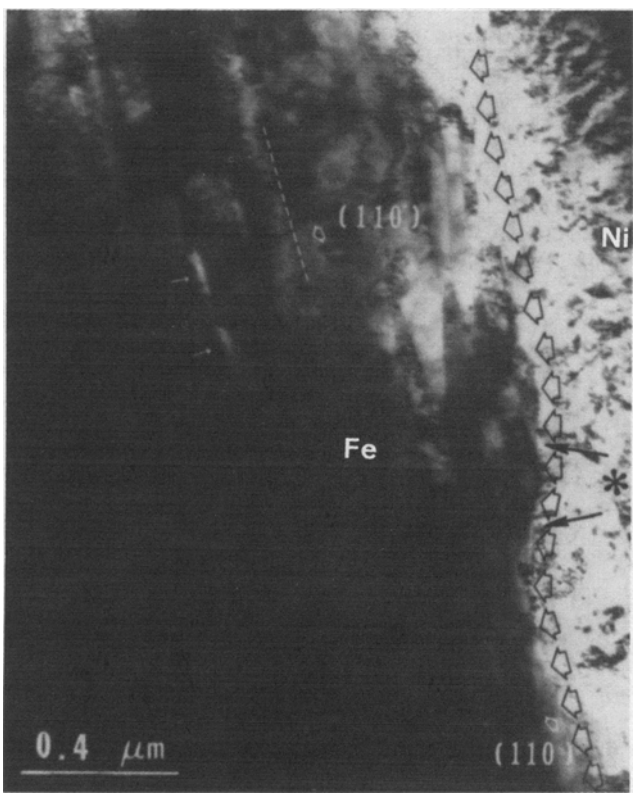

(d)

Fig. 8—Transmission electron micrographs of the profile fractographic specimens showing the fracture surface and subsurface microcracks. (*a*) The fractograph shows the fracture surface (large arrows), a subsurface interlath crack (small arrow), and a subsurface diffraction pattern showing broadened diffraction spots that suggest plastic deformation. (*b*) The fractograph shows the fracture surface (large arrows) and 3 subsurface interlath cracks (small arrows) which are nearly connected. (*c*) The fractograph shows the fracture surface (large arrows), an interlath microcrack (a), and a microcrack within a lath (b) that apparently originates from a carbide particle. (*d*) The fractograph shows the fracture surface (large arrows), apparent translath steps in the fracture surface (*), the trace of the (110) plane, which is sensibly parallel to the fracture surface, and subsurface interlath microcracks (small arrows).

separating twin-related laths are known to be present in the usual microstructure of the alloy.

The results and conclusions reported here do not deny the common hypothesis that hydrogen embrittlement is related to the formation of hydrogen atmospheres around dislocations;[6,14,15] the lath boundaries are highly dislocated, and hydrogen atmospheres will certainly affect their interfacial cohesion. It is also possible that dislocation glide influences the interlath fracture; the embrittled specimens undergo substantial plastic deformation during fracture and, in some cases, the material immediately adjacent to the quasicleavage fracture surface has been significantly deformed. The results seem to establish, however, that classic "glide plane decohesion" is a minor factor in the hydrogen-induced quasicleavage of 5.5Ni steel if it is relevant at all. Moreover, since the quasicleavage is predominantly interfacial, it is not necessary to assume that hydrogen has any relevant effect on the bonding characteristics of the bulk alloy.

While the results reported here refer to a particular alloy and heat treatment, we suspect that they are widely applicable to high strength martensitic steels. The mechanism of hydrogen embrittlement which we have apparently observed is a plausible mechanism in any martensitic steel. The various scanning electron micrographs published by Kikuta and co-workers[1,2,15] seem to show a predominantly lath boundary mode in the transgranular fracture of embrittled martensitic steels. Moreover, the interlath mode will automatically yield a quasicleavage surface which is both irregular on a microscopic scale and dominated by {110} fracture facets, in agreement with common experimental results from a variety of steels.

A similar process seems to operate in Fe-based alloys which contain no martensite phase. For example, Nagumo and co-workers[9] studied the hydrogen embrittlement of pure iron and found that embrittlement occurred only after the iron had been strained sufficiently to form well-defined subgrains. Fracture then proceeded through the nucleation and linkage of microfractures in the subgrain boundaries. In this case also the dominant mechanism of "transgranular" hydrogen embrittlement is apparently interfacial decohesion along internal boundaries.

ACKNOWLEDGMENTS

The authors are grateful to the Nippon Steel Company for supplying the research material and to W. Salesky, Materials and Molecular Research Division, Lawrence Berkeley Laboratory, for assistance in the preparation of the profile fractographic specimens. This research was supported by the Office of Naval Research under Contract No. N00014-75-C-0154, NR 031-762.

REFERENCES

1. Y. Kikuta, T. Araki, and T. Kuroda: *Fractography in Failure Analysis,* B. M. Strauss and W. M. Cullen, Jr., eds., ASTM STP 645, American Society for Testing and Materials, 1978, p. 107.
2. Y. Kikuta and T. Araki: *Hydrogen Effects in Metals,* I. M. Bernstein and A. W. Thompson, eds., TMS-AIME, Warrendale, PA, 1981, p. 309.
3. F. Nakasoto and I. M. Bernstein: *Metall. Trans. A,* 1978, vol. 9A, p. 1317.
4. I. M. Bernstein: *Metall. Trans. A,* 1970, vol. 1, p. 3143.
5. Y. Takeda and C. J. McMahon, Jr.: *Metall. Trans. A,* 1981, vol. 12A, p. 1255.
6. C. J. McMahon, Jr.: *Hydrogen Effects in Metals,* I. M. Bernstein and A. W. Thompson, eds., TMS-AIME, Warrendale, PA, 1981, p. 219.
7. J. I. Kim: Ph.D. Thesis, Department of Materials Science and Mineral Engineering, University of California, Berkeley, CA, 1979.
8. J. I. Kim, C. K. Syn, and J. W. Morris, Jr.: *Metall. Trans. A,* 1983, vol. 14A, p. 93.
9. M. Nagumo, H. Morikawa, and K. Miyamoto: Proceedings JIMIS-2, Hydrogen in Metals, Suppl. Trans. Japan Inst. Metals, 1980, vol. 21, p. 405.
10. H. Haga and H. Mimura: *Trans. Japan Inst. Metals,* 1972, vol. 13, p. 155.
11. C. K. Syn, B. Fultz, and J. W. Morris, Jr.: *Metall. Trans. A,* 1978, vol. 9A, p. 1635.
12. S. Matsuda, T. Inoue, H. Mimura, and Y. Okamura: *Toward Improved Ductility and Toughness,* Climax Molybdenum Development Co. (Japan) Ltd., Kyoto, 1972, p. 45.
13. S. Hogmark, H. Swahn, and O. Vingsbo: *Ultramicroscopy,* 1975, vol. 1, p. 113.
14. J. Tien, S. Nair, and R. Jensen: *Hydrogen Effects in Metals,* I. M. Bernstein and A. W. Thompson, eds., TMS-AIME, Warrendale, PA, 1981, p. 37.
15. Y. Kikuta, *ibid.*, p. 755.